Matter and Radiation at Extremes | RESEARCH ARTICLE | pubs.aip.org/aip/mre

Transition from backward to sideward stimulated Raman scattering with broadband lasers in plasmas

Cite as: Matter Radiat. Extremes 8, 065601 (2023); doi: 10.1063/5.0152668
Submitted: 31 March 2023 • Accepted: 4 August 2023 •
Published Online: 13 September 2023

X. F. Li,[1,2,3,a] S. M. Weng,[1,2,b] P. Gibbon,[3,4] H. H. Ma,[1,2,5] S. H. Yew,[1,2] Z. Liu,[1,2] Y. Zhao,[6] M. Chen,[1,2] Z. M. Sheng,[1,2,5,b] and J. Zhang[1,2,5]

AFFILIATIONS

[1] Key Laboratory for Laser Plasmas (MoE), School of Physics and Astronomy, Shanghai Jiao Tong University, Shanghai 200240, China
[2] Collaborative Innovation Center of IFSA, Shanghai Jiao Tong University, Shanghai 200240, China
[3] Institute for Advanced Simulation, Jülich Supercomputing Centre, Forschungszentrum Jülich, 52425 Jülich, Germany
[4] Centre for Mathematical Plasma Astrophysics, Katholieke Universiteit Leuven, 3000 Leuven, Belgium
[5] Tsung-Dao Lee Institute, Shanghai Jiao Tong University, Shanghai 200240, China
[6] School of Science, Shenzhen Campus of Sun Yat-sen University, Shenzhen 518107, China

[a] **Present address:** State Key Laboratory of High Field Laser Physics and CAS Center for Excellence in Ultra-intense Laser Science, Shanghai Institute of Optics and Fine Mechanics, Chinese Academy of Sciences, Shanghai 201800, China.
[b] **Authors to whom correspondence should be addressed:** wengsuming@sjtu.edu.cn and zmsheng@sjtu.edu.cn

ABSTRACT

Broadband lasers have been proposed as future drivers of inertial confined fusion (ICF) to enhance the laser–target coupling efficiency via the mitigation of various parametric instabilities. The physical mechanisms involved have been explored recently, but are not yet fully understood. Here, stimulated Raman scattering (SRS) as one of the key parametric instabilities is investigated theoretically and numerically for a broadband laser propagating in homogeneous plasma in multidimensional geometry. The linear SRS growth rate is derived as a function of scattering angles for two monochromatic laser beams with a fixed frequency difference $\delta\omega$. If $\delta\omega/\omega_0 \sim 1\%$, with ω_0 the laser frequency, these two laser beams may be decoupled in stimulating backward SRS while remaining coupled for sideward SRS at the laser intensities typical for ICF. Consequently, side-scattering may dominate over backward SRS for two-color laser light. This finding of SRS transition from backward to sideward SRS is then generalized for a broadband laser with a few-percent bandwidth. Particle-in-cell simulations demonstrate that with increasing laser bandwidth, the sideward SRS gradually becomes dominant over the backward SRS. Since sideward SRS is very efficient in producing harmful hot electrons, attention needs to be paid on this effect if ultra-broadband lasers are considered as next-generation ICF drivers.

NOMENCLATURE

a_0	normalized intensity of monochromatic laser
a_i, $i = 1, 2$	normalized intensities in two-color laser beams
$\mathbf{k} = k_x\mathbf{i} + k_y\mathbf{j}$	wave vector of electron plasma wave
$\mathbf{k}_0 = k_0\mathbf{i}$	wave vector of pump laser in plasma
$\mathbf{k}_i = k_i\mathbf{i}$, $i = 1, 2$	wave vectors in two-color laser beams
k_r	wavenumber of electron plasma wave at resonance
$\mathbf{k}_s = k_{sx}\mathbf{i} + k_{sy}\mathbf{j}$	wave vector of scattered light
k_{sr}	wavenumber of scattered light at resonance
Γ	linear growth rate of electron plasma wave
$\Delta k = \sqrt{(k_x - k_0)^2 + k_y^2} - k_{sr}$	deviation in electron plasma wavenumber from resonance point
Δk_b	boundary of Δk at $\Gamma = 0$ for electron plasma wave
$\Delta\omega$	bandwidth of broadband laser

δk_r	difference in electron plasma wavenumber at resonance due to $\delta\omega$
$\delta\omega$	frequency difference in two-color laser beams
$\theta = 180° - \arctan[k_y/(k_x - k_0)]$	scattering angle
$\theta_{\rm th}$	threshold angle of coupling condition
ω_0	frequency of pump laser in plasma
$\omega_i, i = 1, 2$	frequencies in two-color laser beams
ω_{pe}	frequency of electron plasma wave
ω_s	frequency of scattered light

I. INTRODUCTION

Mitigation of parametric instabilities in laser–plasma interactions is crucial for the success of laser-driven inertial confinement fusion (ICF).[1–3] The most important instabilities include stimulated Raman scattering (SRS), stimulated Brillouin scattering (SBS), and two-plasmon decay (TPD),[4,5] which not only inhibit energy deposition by scattering light away from plasmas, but also reduce fuel compressibility owing to the generation of suprathermal electrons.[2,6] Since the 1960s, various laser techniques and schemes have been proposed to mitigate parametric instabilities by increasing the incoherence of the driving lasers, such as beam smoothing,[7–12] temporal shaping,[13] frequency chirping,[14] and using broadband lasers.[15–17]

With the use of broadband lasers,[15–24] the instability growth rate is expected to be reduced by a factor of $\Gamma/\Delta\omega$ when the laser bandwidth $\Delta\omega$ is larger than the linear growth rate Γ of the instabilities.[18] Experiments have demonstrated that SBS can be efficiently suppressed by using spatially and temporally incoherent laser beams.[20] Frequency detuning of the drive laser beams is expected to suppress the TPD instability and hot-electron generation in direct-drive ICF, even with a relatively narrow bandwidth ~0.7%.[22] Numerical simulations have also demonstrated the efficacy of multi-terahertz laser bandwidth in suppressing cross-beam energy transfer in direct-drive ICF.[23] Furthermore, the thresholds of absolute SRS and TPD can be significantly increased when 1% laser bandwidth is introduced for ICF-relevant conditions.[24,25]

SRS, in which a laser light wave decays into an electron plasma wave and a scattered light wave, has received most attention, because it usually has a larger growth rate than other instabilities. Previous studies have shown that broadband lasers can effectively reduce SRS,[16,21,26–28] although the effects of laser bandwidth on the scattering angle of SRS have rarely been studied. In particular, some simulations have revealed that forward SRS could develop when backward SRS is suppressed.[29] Further, sideward SRS with a monochromatic laser beam has been studied extensively,[30–33] and it has been shown that the scattering angle varies with the laser spot size. Importantly, sideward SRS can not only generate hot electrons,[34,35] but also seed instabilities by interacting with other laser beams.[36] Therefore, it becomes particularly important to investigate the angular distributions of SRS when backward SRS may already be suppressed by using a broadband laser.

In this work, the competition between sideward and backward SRS in the interactions between broadband lasers and homogeneous plasmas is investigated theoretically and numerically. Our study suggests that a much larger bandwidth is required to suppress side-scattering as compared to backscattering. The remainder of the paper is organized as follows. In Sec. II, a theoretical model of SRS side-scattering for the coupling of two monochromatic laser beams with a certain frequency difference is presented. Extension to broadband lasers is done by numerical simulations in Sec. III. The paper concludes with a summary in Sec. IV.

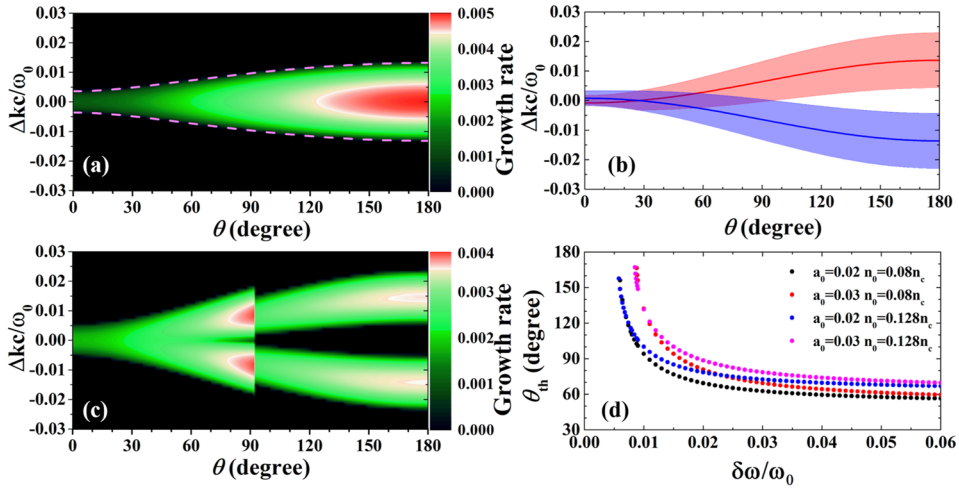

FIG. 1. Linear theory of the SRS growth rate for a two-color laser. (a) Distribution of SRS growth rate Γ calculated according to Eq. (1) with $a_0 = 0.02$ and $n_0 = 0.128n_c$. Here, $\Delta k = \sqrt{(k_x - k_0)^2 + k_y^2} - k_{sr}$ and $\theta = 180° - \arctan[k_y/(k_x - k_0)]$. The resonance point k_{sr} is defined by the wave vector and frequency matching conditions of a monochromatic laser beam. (b) Region for $\Gamma > 0$ as a function of scattering angle (θ) for two individual laser beams at frequencies $\omega_0 \pm 0.5\delta\omega$, denoted by the red and blue regions, respectively. Here, $\delta\omega/\omega_0 = 1.2\%$, and $a_{1,2} = 0.0141$. The solid red and blue lines are the resonance points calculated using Eq. (3), and the width of each instability region is calculated using Eq. (2). (c) Growth rate as a function of scattering angle calculated using Eq. (5) for two-color laser light with $\delta\omega/\omega_0 = 1.2\%$. (d) Coupling threshold angle $\theta_{\rm th}$ as a function of the frequency difference $\delta\omega$ between two individual monochromatic laser beams.

II. THEORY OF TWO-LASER-BEAM COUPLING IN SIDE-SCATTERING

We start from the general dispersion relation for SRS with a monochromatic laser $\mathbf{A}_L = \mathbf{A}_0 \cos(\mathbf{k}_0 \cdot \mathbf{x} - \omega_0 t)$:[37,38]

$$\frac{4(\omega^2 - \omega_{pe}^2)}{\omega_{pe}^2 k^2 c^2 a_0^2} = \frac{1}{D(\mathbf{k} - \mathbf{k}_0, \omega - \omega_0)} + \frac{1}{D(\mathbf{k} + \mathbf{k}_0, \omega + \omega_0)}, \quad (1)$$

where $D(\mathbf{k} \pm \mathbf{k}_0, \omega \pm \omega_0) = (\omega \pm \omega_0)^2 - (k_x \pm k_0)^2 c^2 - k_y^2 c^2 - \omega_{pe}^2$, $\mathbf{k}_0 = k_0 \mathbf{i}$ is the laser wave vector in the plasma, $a_0 = e\mathbf{A}_0/m_e c^2$ is the normalized laser intensity, and $\mathbf{k} = k_x \mathbf{i} + k_y \mathbf{j}$ and ω_{pe} are the wave vector and frequency of the electron plasma wave, respectively. For the sake of simplicity here, the effect of the plasma temperature is ignored in the theoretical model. For backward SRS, $k_y = 0$.[37] For sideward SRS, however, $k_y \neq 0$.

The linear growth rate $\Gamma = \mathrm{Im}(\omega)$ can be obtained from Eq. (1). As an example, this is displayed as a function of the scattering angle θ, defined by $\theta = 180^\circ - \arctan[k_y/(k_x - k_0)] = \arctan(k_{sy}/k_{sx})$, in Fig. 1(a), where $a_0 = 0.02$ and $n_0 = 0.128 n_c$, and k_{sx} and k_{sy} are the two components of $\mathbf{k}_s$. Combining Eq. (1) with the frequency and wave vector matching conditions between the pump laser $(\omega_0, \mathbf{k}_0)$, the scattered light $(\omega_s, \mathbf{k}_s)$, and the electron plasma wave $(\omega_{pe}, \mathbf{k})$, one can obtain $k_{sr} = 0.533\,\omega_0/c$ and $\omega_s = 0.642\,\omega_0$ at the resonance point for a cold plasma.

The probability distribution of the electron plasma wave vector $\mathbf{k}$ at resonance is a circle of radius $k_{sr} = 0.533\,\omega_0/c$ and center at $k_0 = 0.934\,\omega_0/c$, and the maximum growth rate $\Gamma_{\max}$ is obtained for backward SRS with $\theta = 180^\circ$. For a monochromatic laser, the growth rate Γ decreases monotonically with decreasing scattering angle θ.

SRS can develop within certain region around the resonance points, the boundary of which is sketched by the dashed lines in Fig. 1(a). Here, polar coordinates are used, where the center is the resonance point $k_{sr} = 0.533\omega_0/c$, and $\Delta k = \sqrt{(k_x - k_0)^2 + k_y^2} - k_{sr}$ is the deviation of the wavenumber of the electron plasma wave from the resonance point. The boundary can be obtained from Eq. (1) using $\Gamma = 0$ as

$$\Delta k_b = a_0 k_r \sqrt{\frac{\omega_{pe}(\omega_0 - \omega_{pe})}{\omega_0^2 - 2\omega_0 \omega_{pe}}}, \quad (2)$$

where $k_r = \sqrt{k_0^2 + k_{sr}^2 - 2k_0 k_{sr} \cos\theta}$ is the wavenumber of the electron plasma wave at the resonance points.

We now consider a broadband laser, which can be considered as the superposition of many monochromatic lasers with different frequencies. To simplify the analysis, we first consider the case with two monochromatic laser beams at frequencies $\omega_0 \pm 0.5\delta\omega$. These two beams have their own resonance points with the electron plasma waves of different wavenumbers $k_r \pm 0.5\delta k_r$, where the wavenumber difference δk_r can be evaluated as

$$\frac{\delta k_r}{\delta \omega_0} \approx \frac{dk_{rx}}{d\omega_0} = \frac{\omega_0}{c\sqrt{\omega_0^2 - \omega_{pe}^2}} - \frac{(\omega_0 - \omega_{pe})\cos\theta}{c\sqrt{\omega_0^2 - 2\omega_{pe}\omega_0}}, \quad (3)$$

where the electron plasma wave component along the x direction, k_{rx}, is given by

$$k_{rx} = c^{-1}\left(\sqrt{\omega_0^2 - \omega_{pe}^2} - \cos\theta\sqrt{\omega_0^2 - 2\omega_{pe}\omega_0}\right). \quad (4)$$

Analogous to Eq. (1), the dispersion relation for this two-color laser light with $\mathbf{A}_L = \mathbf{A}_1 \cos(\mathbf{k}_1 \cdot \mathbf{x} - \omega_1 t) + \mathbf{A}_2 \cos(\mathbf{k}_2 \cdot \mathbf{x} - \omega_2 t)$ can be obtained as

$$\omega^2 - \omega_{pe}^2 = \frac{k^2 c^2 \omega_{pe}^2}{4}[\Pi_0 + f(\theta)\Pi_\times], \quad (5a)$$

where

$$\Pi_0 = \sum_{i=1}^{2}\left[\frac{a_i^2}{D(\mathbf{k} + \mathbf{k}_i, \omega + \omega_i)} + \frac{a_i^2}{D(\mathbf{k} - \mathbf{k}_i, \omega - \omega_i)}\right], \quad (5b)$$

$$\Pi_\times = \sum_{i=1}^{2}\left[\frac{a_1 a_2}{D(\mathbf{k} + \mathbf{k}_i, \omega + \omega_i)} + \frac{a_1 a_2}{D(\mathbf{k} - \mathbf{k}_i, \omega - \omega_i)}\right]. \quad (5c)$$

Here, Π_0 is the direct contribution of two individual monochromatic laser beams, while $\Pi_\times$ is the contribution caused by the coupling of these two beams. The coupling factor $f(\theta)$ is a function of the scattering angle, which depends on the frequency difference $\delta\omega$ and other laser–plasma parameters. The derivation of the above dispersion relation is detailed in Appendix A.

To examine the coupling condition, let us consider the two-color light case with $\delta\omega/\omega_0 = 1.2\%$, $a_{1,2} = 0.0141$, and $n_0 = 0.128 n_c$. In Fig. 1(b), the resonance points obtained from Eq. (3) for two individual monochromatic beams are shown by the red and blue lines, respectively, while the instability regions with $\Gamma > 0$ obtained from Eq. (2) are shown by the red and blue shading, respectively. If these two instability regions overlap, then these two beams couple with each other and $f(\theta) = 1$. Otherwise, the two beams are decoupled and $f(\theta) = 0$. Figure 1(b) indicates that the two instability regions overlap when the scattering angle θ is less than a certain angle θ_{th}. This threshold θ_{th} can be evaluated using Eqs. (2) and (3) as

$$\Delta k_b(\theta_{\mathrm{th}}) = \delta k_r(\theta_{\mathrm{th}}). \quad (6)$$

Correspondingly, the coupling factor is

$$f(\theta) = \begin{cases} 1, & \theta < \theta_{\mathrm{th}}, \\ 0, & \theta \geq \theta_{\mathrm{th}}. \end{cases} \quad (7)$$

For convenience, the notation used in the derivation of the theoretical model has been summarized in the Nomenclature list at the start of the paper. For given electron density and laser intensity, Fig. 1(d) shows that θ_{th} decreases with increasing frequency difference $\delta\omega$. As shown in Fig. 1(b), one has $\theta_{\mathrm{th}} \simeq 90^\circ$ for $\delta\omega/\omega_0 = 1.2\%$, $a_{1,2} = 0.0141$, and $n_0 = 0.128\,n_c$. By combining Eqs. (5) and (7), the growth rate Γ for two-color laser light can be calculated numerically. As shown in Fig. 1(c), it is now found that the maximum value of Γ is achieved at $\theta \simeq \theta_{\mathrm{th}} \simeq 90^\circ$, and so sideward SRS will dominate over backward SRS. In other words, stimulated side-scattering can develop even if backscattering is suppressed by using two-color laser light.

For the sake of simplicity, the coupling factor in Eq. (5) is set to be $f(\theta) = 1$ if these two laser beams are coupled. Otherwise, $f(\theta) = 0$. Such a step function form of the coupling factor $f(\theta)$ induces a discontinuity in the growth rate as shown in Fig. 1(c). In reality, however, the growth rate may not drop so suddenly if the transition from coupling to decoupling takes place in a finite region.

The above analysis was carried out for two different monochromatic laser beams, but it can in principle be extended to many

monochromatic laser beams at different frequencies. On the other hand, broadband laser light can be considered as the superposition of many monochromatic laser beams. Therefore, the phenomenon discussed above, namely, the development of sideward SRS and its dominance over backward SRS, is expected to arise with a broadband laser as well. In the case of a broadband laser with a continuous frequency spectrum, however, the transition from backward to sideward SRS will take place at a fractional bandwidth that is different from the required frequency difference in the theoretical analysis using two-color laser beam.

III. SIMULATION RESULTS AND DISCUSSION

To verify the above analysis, a series of 2D simulations were carried out by using the particle-in-cell (PIC) code EPOCH.[39] The laser was incident along the x direction, with a Gaussian profile in the transverse direction. The laser wavelength $\lambda = 0.35\ \mu$m, the spot size $w_0 = 10\lambda$, and the normalized amplitude $a_0 = 0.02$. A semi-infinite pulse was adopted, with a linear ramp at the initial 60 fs. The simulation box was $110\lambda \times 40\lambda$ and was resolved with a cell dimension of $dx \times dy = 0.02\lambda \times 0.05\lambda$. There were 100 macroparticles per species per cell, and absorbing boundary conditions were used along each direction. The initial electron temperature was $T_e = 3$ keV, and the ions were fixed. Since side-scattering preferentially occurs out of the polarization plane,[37] S-polarized laser fields were assumed in the simulations.

For comparison, we first show the spatial distribution of E_x at $t = 800T_0$ with a monochromatic laser beam in Fig. 2(a). It can be seen that the scattering due to SRS is largely concentrated around $\theta = 180°$. The wave-vector distribution of E_x integrated over $0 \le t \le 1500T_0$ is plotted in Fig. 2(b), which demonstrates that the scattering has its maximum amplitude roughly at $\theta_{peak} = 180°$. This confirms that backward SRS is the dominant scattering for a monochromatic laser beam.

For comparison, the integrated wave-vector distributions of E_x for two-color laser light with $\delta\omega/\omega_0 = 0.6\%$ and 1.2% are shown in Figs. 2(c) and 2(d), respectively. Here, the amplitudes of two individual monochromatic laser beams are set to be $a_1 = a_2 = a_0/\sqrt{2} = 0.0141$, so that their total laser energy is equal to that in the case of a single monochromatic laser beam. As observed in previous studies,[16,21,40] Fig. 2(c) indicates that the backward SRS is significantly reduced when two-color laser light is used. More importantly, Fig. 2(d) demonstrates that significant sideward SRS occurs at roughly $\theta \approx 90°$, whereas backward SRS is effectively suppressed by the use of two-color laser light with $\delta\omega/\omega_0 = 1.2\%$. This phe-

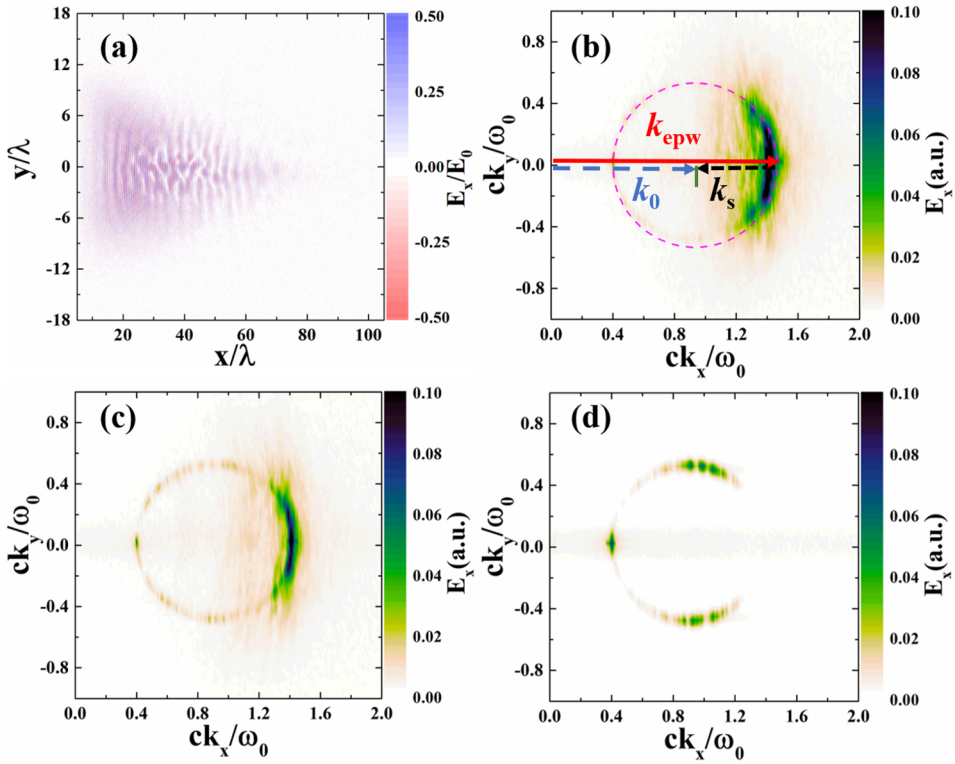

FIG. 2. SRS in the cases of monochromatic and two-color lasers with S-polarization. (a) Spatial distribution of E_x at $800T_0$. (b) Wave-vector distribution of E_x integrated over $0 \le t \le 1500T_0$ for monochromatic laser with S-polarization. Here, $a_0 = 0.02$, $w_0 = 10\lambda$, and $n_0 = 0.128n_c$. (c) and (d) Integrated wave-vector distributions for E_x (S-polarized laser) before $1500T_0$ in cases with two different laser frequencies, $\delta\omega/\omega_0 = 0.6\%$ and $\delta\omega/\omega_0 = 1.2\%$, respectively. The amplitudes of the two beamlets are $a_1 = 0.0141$ and $a_2 = 0.0141$.

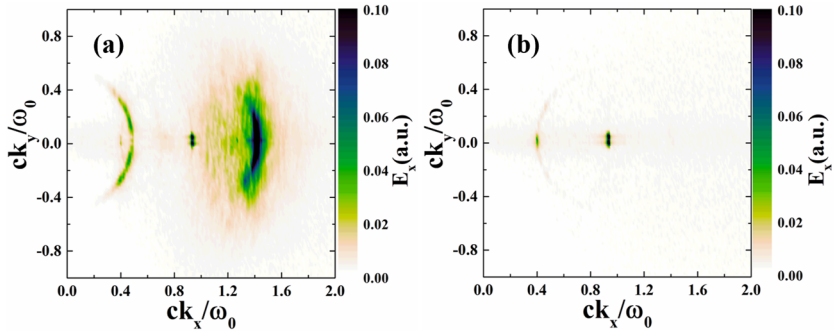

FIG. 3. SRS in the cases of monochromatic and two-color lasers with P-polarization: integrated wave-vector distributions for E_x (P-polarized laser) over $0 \le t \le 1500\ T_0$ in the case of (a) a monochromatic laser and (b) a two-color laser with $\delta\omega/\omega_0 = 1.2\%$.

nomenon is consistent with the theoretical prediction shown in Fig. 1.

We also performed PIC simulations to study the angular distribution of SRS with three-color S-polarized laser light. In this case, the transition from backward to sideward SRS is also observed with increasing frequency difference between individual monochromatic laser beams. In addition, we studied the angular distribution of SRS for the P-polarized case. Figure 3(a) shows that backward SRS is also dominant for a P-polarized monochromatic laser beam. For P-polarized two-color laser light with $\delta\omega/\omega_0 = 1.2\%$, Fig. 3(b)

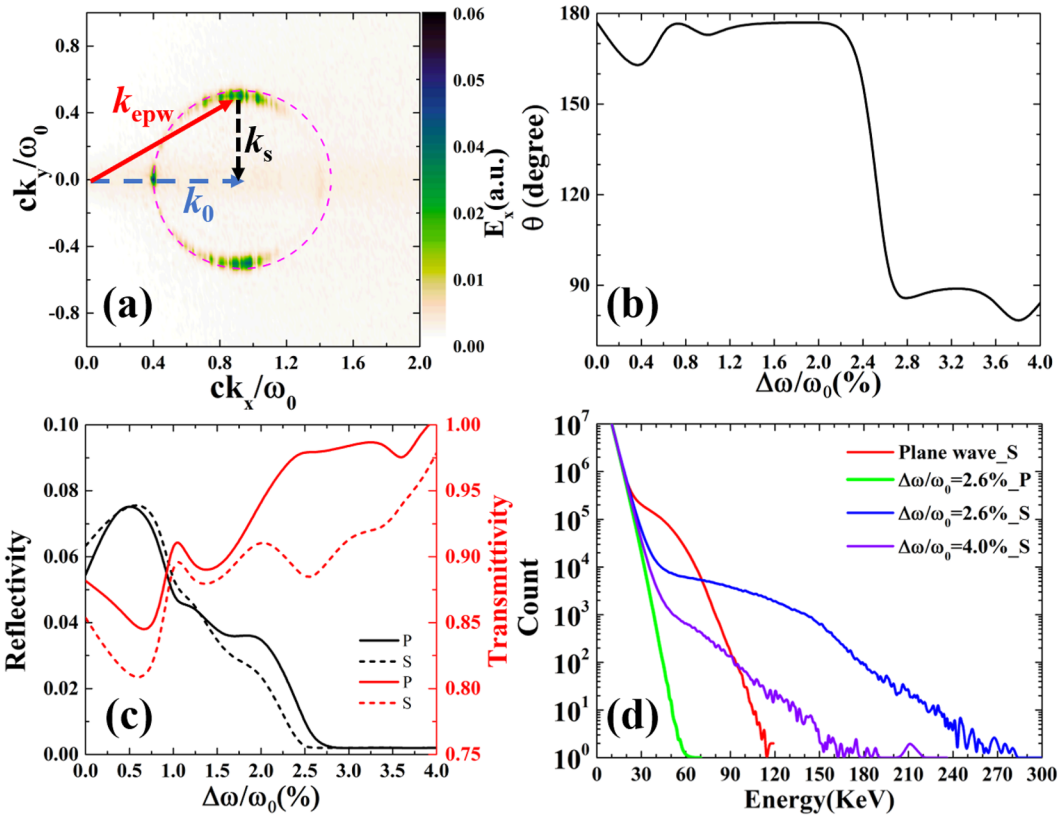

FIG. 4. SRS generated by a broadband laser. (a) Integrated wave-vector distribution for E_x over $0 \le t \le 1500T_0$ for the case of an S-polarized broadband laser with $\Delta\omega/\omega_0 = 2.6\%$. (b) Scattering angle θ with the maximum amplitude as a function of bandwidth. (c) Average reflectivity and transmittivity and (d) electron energy spectrum at $2500T_0$ for broadband lasers with different bandwidths and polarizations.

shows that backward SRS is effectively suppressed. However, no obvious sideward SRS is observed in any of the 2D simulations with P-polarized two-color laser light that we performed, suggesting that sideward SRS is azimuthally anisotropic and preferentially occurs out of the plane of polarization.

Figure 4 demonstrates the transition from backward to sideward SRS when a generalized broadband laser source is used. In these simulations, the broadband laser light was assumed to have a flat-top frequency spectrum, and it was modeled as a combination of an ensemble of monochromatic laser beams[25] (see Appendix B). The energy of the broadband laser was the same as that of the monochromatic laser, and the other simulation parameters were the same as those in Fig. 2.

As expected, the backward SRS is weakened with increasing laser bandwidth $\Delta\omega$. Figure 4(a) indicates that backward SRS is already suppressed effectively by a broadband laser with $\Delta\omega/\omega_0 = 2.6\%$. However, sideward SRS obviously develops around $\theta_{peak} \approx 90°$. The angle θ_{peak} at which the scattering amplitude peaks is shown as a function of $\Delta\omega$ in Fig. 4(b), which clearly illustrates the transition from backward to sideward SRS with increasing laser bandwidth. The averaged reflectivity and transmittivity shown in Fig. 4(c) also reveal the transition from backward to sideward SRS with increasing laser bandwidth. At $\Delta\omega/\omega_0 = 2.6\%$, the reflectivity is nearly zero for both S- and P-polarized laser light, i.e., backward SRS has been effectively suppressed, regardless of polarization. However, there is a noticeable gap between the transmittivities of the P-polarized (~100%) and S-polarized (~87%) broadband sources. The lost laser energy in the case of S-polarization is due to side-scatter, whereas the latter cannot occur with P-polarization in 2D simulations. Interestingly, we find that the reflectivity at $\Delta\omega/\omega_0 \sim 0.5\%$ is higher than that in the monochromatic laser case. This may be caused by the coupling effect in the linear stage, as well as the burst behavior in the nonlinear stage.[41]

In addition, Fig. 4(d) shows that sideward SRS is very efficient at generating harmful hot electrons. Generally, the use of broadband lasers tends to reduce hot electron generation via suppression of backward SRS, as shown for the two cases with $\Delta\omega/\omega_0 = 2.6\%$ for P-polarized and S-polarized lasers. However, the number of hot electrons with kinetic energy $E_k > 80$ keV is much higher in the case of S-polarized broadband lasers, owing to transition of the predomi-

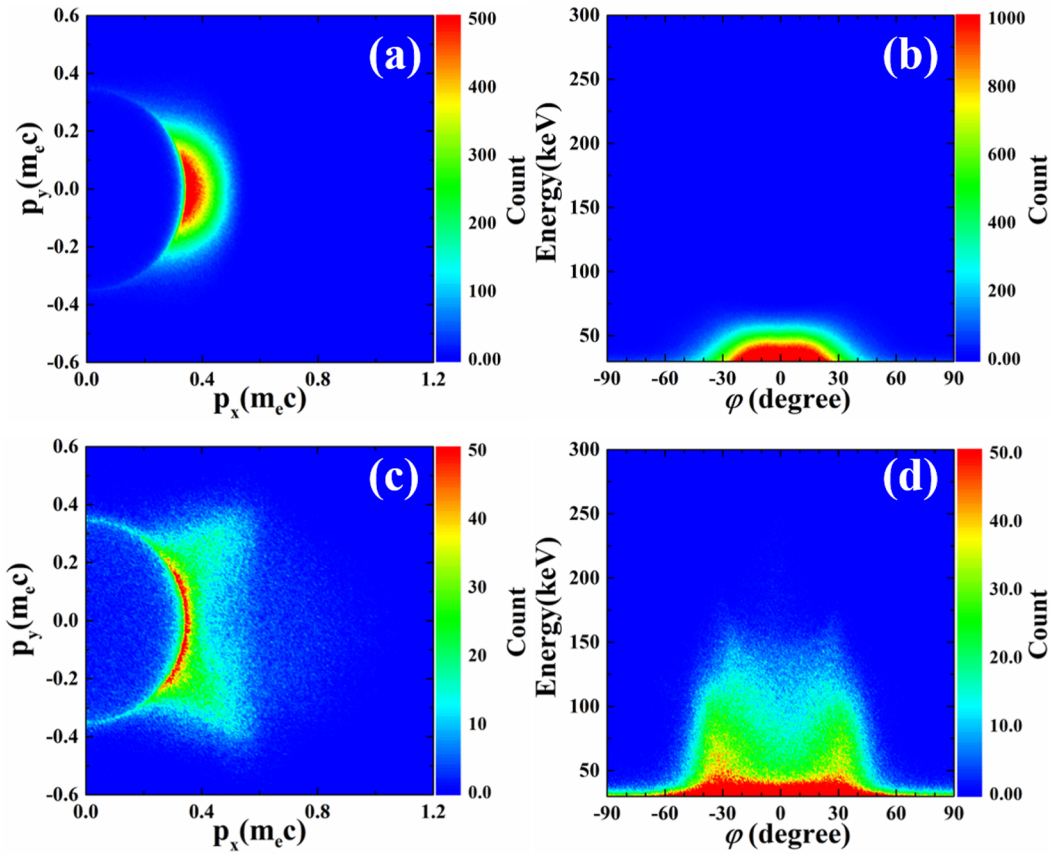

FIG. 5. Hot electron generation with a broadband laser: p_x–p_y phase distributions [(a) and (c)] and energy–angle distributions [(b) and (d)] of hot electrons with kinetic energy $E_k > 30$ keV at $t = 2500\ T_0$ obtained from 2D PIC simulation for the cases of monochromatic laser light [(a) and (b)] and broadband laser light with $\Delta\omega/\omega_0 = 2.6\%$ [(c) and (d)]. Here, $\varphi_i = \arctan(p_{iy}/p_{ix})$, and i labels the individual electrons. The other simulation parameters were the same as those in Fig. 4(a).

nant scattering angle θ from 180°to 90°. This can also be seen in momentum phase space, as presented in Fig. 5. Further, owing to the occurrence of forward SRS as shown in Fig. 4(a), some electrons can attain kinetic energies $E_k > 150$ keV. The efficient hot electron generation due to sideward SRS in the S-polarization case can be partly alleviated with a larger bandwidth $\Delta\omega/\omega_0 = 4.0\%$.

To better understand this, the hot electron distributions in the p_x–p_y phase space are displayed in Figs. 5(a) and 5(c) for monochromatic laser light and broadband laser light with $\Delta\omega/\omega_0 = 2.6\%$, respectively. It is found that the hot electrons generated by monochromatic laser light are roughly collimated along the laser axis, whereas those generated by broadband laser light diverge significantly from the laser axis. The corresponding energy–angle distributions of the hot electrons with kinetic energies $E_k > 30$ keV are compared in Figs. 5(b) and 5(d). It is clear that broadband laser light is more efficient in generating hot electrons with kinetic energies $E_k > 80$ keV and that these more energetic hot electrons are mainly distributed along directions roughly at ±30° with respect to the laser axis. Such an angular distribution of hot electrons with higher energies is closely related to the direction of the plasma wave vector $\mathbf{k}_{epw}$ stimulated by the broadband laser light, as shown in Fig. 4(a). More importantly, the plasma wave of the sideward SRS in the broadband laser case has a smaller wavenumber k_{epw} than that of the backward SRS in the monochromatic laser case, as can be seen in Figs. 2(b) and 4(a). Correspondingly, the plasma wave phase velocity ω_{epw}/k_{epw} of the sideward SRS stimulated by the broadband laser is higher than that of the backward SRS stimulated by the monochromatic laser. Consequently, the hot electrons generated by the broadband laser with $\Delta\omega/\omega_0 = 2.6\%$ are more energetic.

For the sake of simplicity, Landau damping has been ignored in our theoretical model. However, it is worth pointing out that Landau damping depends strongly on the ratio of plasma wave phase velocity to electron thermal velocity. Consequently, it will be affected significantly by the scattering direction. That is to say, the Landau damping rates of obliquely propagating electron plasma waves will be smaller than those for backward SRS. Considering Landau damping, therefore, the threshold of backward SRS will be enhanced more obviously than that of sideward SRS. The influence of Landau damping on the competition between backward and sideward scattering will be studied in more detail in future work. In addition, the amplification of the side-scattered light may be suppressed with the use of a finite laser spot, because they propagate out from the laser beam axis.[42] With an infinite laser spot, sideward SRS would become stronger and surpass backward SRS with a smaller laser bandwidth.

Moreover, in this study, the SRS is mainly discussed in the context of interaction of a broadband laser and a homogeneous plasma. In an inhomogeneous plasma, the sideward SRS at angles near 90° has the lowest threshold, owing to the largest resonant region being along the transverse direction. This threshold at densities below $n_c/4$ can increase with increasing laser bandwidth.[43] Experiments with normal lasers at intensities relevant to shock ignition schemes have shown that sideward SRS cannot be ignored, since it not only scatters laser energy at large angles, but also damps TPD and backward SRS driven in the higher-density region.[44,45] Therefore, there is a need for further study of the competition between sideward SRS, backward SRS, and TPD in the region close to $n_c/4$.

IV. SUMMARY

In conclusion, we have found that the angular distribution of SRS depends strongly on laser bandwidth. First, the growth rate of SRS has been derived as a function of the scattering angle for two-color laser light at frequencies $\omega_0 \pm 0.5\delta\omega$. It is found that the two frequency components will be decoupled when the scattering angle is larger than a threshold angle θ_{th}, which decreases with increasing $\delta\omega$. Consequently, the strongest growing SRS will not always be located at $\theta = 180°$. It turns out that sideward SRS may dominate over backward SRS for two-color laser light, as demonstrated by numerical simulation. Second, the transition from backward to sideward SRS has been confirmed generally for broadband lasers, which can be considered as the superposition of many monochromatic laser beams. Because sideward SRS can generate hot electrons with higher energy than backward SRS, special attention should be paid to sideward SRS when broadband lasers are considered as future ICF drivers.[46,47]

ACKNOWLEDGMENTS

This work was supported by the Strategic Priority Research Program of the Chinese Academy of Sciences (Grant No. XDA25050100), the National Natural Science Foundation of China (Grant Nos. 11991074, 11975154, 12005287, and 12135009), and the Science Challenge Project (Grant No. TZ2018005). X. F. Li was supported by the China and Germany Postdoctoral Exchange Program from the Office of the China Postdoctoral Council and the Helmholtz Centre (Grant No. 20191016) and the China Postdoctoral Science Foundation (Grant No. 2018M641993). Y. Zhao was also supported by Guangdong Basic and Applied Basic Research Foundation (Grant No. 2023A1515011695). Simulations were carried out on the JURECA and JUWELS supercomputers at the Jülich Supercomputing Centre, which are granted from the Projects JZAM04 and LAPIPE.

AUTHOR DECLARATIONS

Conflict of Interest

The authors have no conflicts to disclose.

Author Contributions

X. F. Li: Data curation (lead); Formal analysis (lead); Methodology (equal); Visualization (lead); Writing – original draft (lead). **S. M. Weng**: Conceptualization (lead); Supervision (equal); Validation (lead); Writing – review & editing (equal). **P. Gibbon**: Writing – review & editing (equal). **H. H. Ma**: Software (equal); Writing – review & editing (equal). **S. H. Yew**: Writing – review & editing (equal). **Z. Liu**: Data curation (equal); Writing – review & editing (equal). **Y. Zhao**: Data curation (equal); Writing – review & editing (equal). **M. Chen**: Writing – review & editing (equal). **Z. M. Sheng**: Conceptualization (equal); Supervision (equal); Validation (equal); Writing – review & editing (equal). **J. Zhang**: Writing – review & editing (equal).

DATA AVAILABILITY

The data that support the findings of this study are available from the corresponding author upon reasonable request.

APPENDIX A: DISPERSION RELATION FOR SRS WITH A TWO-COLOR LASER

In the mutual electromagnetic field of two laser beams,

$$\begin{aligned}\mathbf{A}_L &= \mathbf{A}_1 \cos(\mathbf{k}_1\cdot\mathbf{x}-\omega_1 t) + \mathbf{A}_2 \cos(\mathbf{k}_2\cdot\mathbf{x}-\omega_2 t)\\ &= \frac{1}{2}\mathbf{A}_1\left[e^{i(\mathbf{k}_1\cdot\mathbf{x}-\omega_1 t)} + e^{-i(\mathbf{k}_1\cdot\mathbf{x}-\omega_1 t)}\right]\\ &\quad + \frac{1}{2}\mathbf{A}_2\left[e^{i(\mathbf{k}_2\cdot\mathbf{x}-\omega_2 t)} + e^{-i(\mathbf{k}_2\cdot\mathbf{x}-\omega_2 t)}\right],\end{aligned} \tag{A1}$$

the three-wave coupling equations can be obtained from a Fourier analysis as

$$\begin{aligned}&(\omega^2 - c^2k^2 - \omega_{pe}^2)\mathbf{A}_s(\mathbf{k},\omega)\\ &\quad = \frac{4\pi e^2}{2m_e}\mathbf{A}_1[\delta n(\mathbf{k}+\mathbf{k}_1,\omega+\omega_1) + \delta n(\mathbf{k}-\mathbf{k}_1,\omega-\omega_1)]\\ &\quad\quad + \frac{4\pi e^2}{2m_e}\mathbf{A}_2[\delta n(\mathbf{k}+\mathbf{k}_2,\omega+\omega_2) + \delta n(\mathbf{k}-\mathbf{k}_2,\omega-\omega_2)],\end{aligned} \tag{A2}$$

$$\begin{aligned}&(\omega^2 - 3v_e^2k^2 - \omega_{pe}^2)\delta n(\mathbf{k},\omega)\\ &\quad = \frac{n_0e^2k^2}{2m_e{}^2c^2}\mathbf{A}_1[\mathbf{A}_s(\mathbf{k}+\mathbf{k}_1,\omega+\omega_2) + \mathbf{A}_s(\mathbf{k}-\mathbf{k}_1,\omega-\omega_1)]\\ &\quad\quad + \frac{n_0e^2k^2}{2m_e{}^2c^2}\mathbf{A}_2[\mathbf{A}_s(\mathbf{k}+\mathbf{k}_2,\omega+\omega_2) + \mathbf{A}_s(\mathbf{k}-\mathbf{k}_2,\omega-\omega_2)].\end{aligned} \tag{A3}$$

From Eq. (A2), we obtain

$$\begin{aligned}&\mathbf{A}_s(\mathbf{k}+\mathbf{k}_1,\omega+\omega_1)\\ &\quad = \frac{4\pi e^2}{2m_e}\frac{\mathbf{A}_1\delta n(\mathbf{k},\omega) + \mathbf{A}_2\delta n(\mathbf{k}+\mathbf{k}_1-\mathbf{k}_2,\omega+\omega_1-\omega_2)}{D(\mathbf{k}+\mathbf{k}_1,\omega+\omega_1)},\end{aligned} \tag{A4}$$

where $D(\mathbf{k},\omega) = \omega^2 - k^2c^2 - \omega_{pe}^2$, and the terms $\delta n(\mathbf{k}+\mathbf{k}_1+\mathbf{k}_2, \omega+\omega_1+\omega_2)$ and $\delta n(\mathbf{k}+2\mathbf{k}_1, \omega+2\omega_1)$ are ignored as nonresonant terms. On defining $\Delta\mathbf{k} = \mathbf{k}_1 - \mathbf{k}_2$ and $\Delta\omega = \omega_1 - \omega_2$, we can rewrite Eq. (A4) as

$$\mathbf{A}_s(\mathbf{k}+\mathbf{k}_1,\omega+\omega_1) = \frac{4\pi e^2}{2m_e}\frac{\mathbf{A}_1\delta n(\mathbf{k},\omega) + \mathbf{A}_2\delta n(\mathbf{k}+\Delta\mathbf{k},\omega+\Delta\omega)}{D(\mathbf{k}+\mathbf{k}_1,\omega+\omega_1)}. \tag{A5}$$

Using the same method, we also obtain

$$\mathbf{A}_s(\mathbf{k}-\mathbf{k}_1,\omega-\omega_1) = \frac{4\pi e^2}{2m_e}\frac{\mathbf{A}_1\delta n(\mathbf{k},\omega) + \mathbf{A}_2\delta n(\mathbf{k}-\Delta\mathbf{k},\omega-\Delta\omega)}{D(\mathbf{k}-\mathbf{k}_1,\omega-\omega_1)}, \tag{A6}$$

$$\mathbf{A}_s(\mathbf{k}+\mathbf{k}_2,\omega+\omega_2) = \frac{4\pi e^2}{2m_e}\frac{\mathbf{A}_2\delta n(\mathbf{k},\omega) + \mathbf{A}_1\delta n(\mathbf{k}-\Delta\mathbf{k},\omega-\Delta\omega)}{D(\mathbf{k}+\mathbf{k}_2,k+\omega_2)}, \tag{A7}$$

$$\mathbf{A}_s(\mathbf{k}-\mathbf{k}_2,\omega-\omega_2) = \frac{4\pi e^2}{2m_e}\frac{\mathbf{A}_2\delta n(\mathbf{k},\omega) + \mathbf{A}_1\delta n(\mathbf{k}+\Delta\mathbf{k},\omega+\Delta\omega)}{D(\mathbf{k}-\mathbf{k}_2,\omega-\omega_2)}. \tag{A8}$$

Substituting Eqs. (A5)–(A8) into Eq. (A3), we obtain

$$(\omega^2 - 3v_e^2k^2 - \omega_{pe}^2)\delta n(\mathbf{k},\omega) = \frac{n_0e^2k^2}{2m_e{}^2c^2}\frac{4\pi e^2}{2m_e}\Xi, \tag{A9}$$

where

$$\begin{aligned}\Xi = &\frac{\mathbf{A}_1^2\delta n(\mathbf{k},\omega)}{D(\mathbf{k}+\mathbf{k}_1,\omega+\omega_1)} + \frac{\mathbf{A}_1^2\delta n(\mathbf{k},\omega)}{D(\mathbf{k}-\mathbf{k}_1,\omega-\omega_1)}\\ &+ \frac{\mathbf{A}_2^2\delta n(\mathbf{k},\omega)}{D(\mathbf{k}+\mathbf{k}_2,\omega+\omega_2)} + \frac{\mathbf{A}_2^2\delta n(\mathbf{k},\omega)}{D(\mathbf{k}-\mathbf{k}_2,\omega-\omega_2)}\\ &+ \frac{\mathbf{A}_1\mathbf{A}_2\delta n(\mathbf{k}+\Delta\mathbf{k},\omega+\Delta\omega)}{D(\mathbf{k}+\mathbf{k}_1,\omega+\omega_1)} + \frac{\mathbf{A}_1\mathbf{A}_2\delta n(\mathbf{k}-\Delta\mathbf{k},\omega-\Delta\omega)}{D(\mathbf{k}-\mathbf{k}_1,\omega-\omega_1)}\\ &+ \frac{\mathbf{A}_1\mathbf{A}_2\delta n(\mathbf{k}-\Delta\mathbf{k},\omega-\Delta\omega)}{D(\mathbf{k}+\mathbf{k}_2,\omega+\omega_2)} + \frac{\mathbf{A}_1\mathbf{A}_2\delta n(\mathbf{k}+\Delta\mathbf{k},\omega+\Delta\omega)}{D(\mathbf{k}-\mathbf{k}_2,\omega-\omega_2)}.\end{aligned} \tag{A10}$$

In the coupling case, we can assume that $\delta n(\mathbf{k}\pm\Delta\mathbf{k},\omega\pm\Delta\omega) \simeq \delta n(\mathbf{k},\omega)$. Consequently, Eq. (A9) can be greatly simplified to give the following dispersion relation:

$$\omega^2 - 3v_e^2k^2 - \omega_{pe}^2 = \frac{k^2c^2\omega_{pe}^2}{4}(\Pi_0 + \Pi_\times), \tag{A11a}$$

where

$$\begin{aligned}\Pi_0 = &a_1^2\left[\frac{1}{D(\mathbf{k}+\mathbf{k}_1,\omega+\omega_1)} + \frac{1}{D(\mathbf{k}-\mathbf{k}_1,\omega-\omega_1)}\right]\\ &+ a_2^2\left[\frac{1}{D(\mathbf{k}+\mathbf{k}_2,\omega+\omega_2)} + \frac{1}{D(\mathbf{k}-\mathbf{k}_2,\omega-\omega_2)}\right],\end{aligned} \tag{A11b}$$

$$\begin{aligned}\Pi_\times = &a_1a_2\left[\frac{1}{D(\mathbf{k}+\mathbf{k}_1,\omega+\omega_1)} + \frac{1}{D(\mathbf{k}-\mathbf{k}_1,\omega-\omega_1)}\right.\\ &\left.+ \frac{1}{D(\mathbf{k}+\mathbf{k}_2,\omega+\omega_2)} + \frac{1}{D(\mathbf{k}-\mathbf{k}_2,\omega-\omega_2)}\right],\end{aligned} \tag{A11c}$$

and $a_i = e\mathbf{A}_i/m_ec^2$ and $\omega_{pe} = \sqrt{4\pi e^2n_0/m_e}$.

It is worth noting that $\Pi_\times$ is the contribution caused by the coupling of these two beams. In the decoupling scenario, the density perturbation terms $\delta n(\mathbf{k}\pm\Delta\mathbf{k},\omega\pm\Delta\omega)$ may cancel each other out. On the other hand, these terms may become ignorable as nonresonant terms in comparison with the term $\delta n(\mathbf{k},\omega)$. Therefore, Eq. (A11a) can be approximated as

$$\omega^2 - 3v_e^2k^2 - \omega_{pe}^2 = \frac{k^2c^2\omega_{pe}^2}{4}\Pi_0. \tag{A12}$$

Ignoring the temperature effect, we can combine Eqs. (A11a)–(A11c) and (A12) into the general form of Eqs. (5a)–(5c) in the theoretical model.

For two monochromatic laser beams at frequencies $\omega_{1,2} = \omega_0 \pm 0.5\delta\omega$, these two beams can be considered to be coupled when their instability regions with $\Gamma > 0$ overlap as shown in Fig. 1(b). Otherwise, the two laser beams can be considered to be decoupled.

APPENDIX B: MODEL OF BROADBAND LASER LIGHT

In general, a broadband laser beam can be modeled as a summation of many monochromatic laser beams that have different carrier frequencies ω_i within a given bandwidth $\Delta\omega$ as follows:[16,22–24]

$$E(t) = \sum_{i=0}^{N} E_i \cos(\omega_i t + \psi_i), \tag{B1}$$

where E_i and ω_i are respectively the electric field amplitude and frequency of the ith monochromatic laser beam, and ψ_i is the random phase. If the number of monochromatic laser beams N is chosen arbitrarily, however, the frequency spectrum of the broadband laser electric field modeled in this way will deviate from the initially assumed distribution.[25]

To precisely model the electric field of a broadband laser light, we have employed a novel method by taking the inverse Fourier transform of the amplitude–phase frequency spectrum.[25] Assuming that the broadband laser light has a continuous amplitude frequency spectrum $f(\omega)$, we can construct its amplitude–phase frequency spectrum $F(\omega)$ as the following complex function:

$$F(\omega) = f(\omega)\exp[i\psi(\omega)], \tag{B2}$$

where the phase–frequency spectrum $\psi(\omega)$ varying within $-\pi < \psi < \pi$ is a random function of the frequency ω. Using this amplitude–phase frequency spectrum, we can obtain the electric field $E(t)$ of a broadband laser in the time domain as

$$E(t) = \mathcal{F}^{-1}[F(\omega)], \tag{B3}$$

where $\mathcal{F}^{-1}$ denotes the inverse Fourier transform of a complex function. Actually, the electric field defined by Eq. (B3) is equivalent to that defined by Eq. (B1) if the number of monochromatic laser beams is chosen as $N = T\Delta\omega$, where T and $\Delta\omega$ are the duration and bandwidth of the broadband laser beam, respectively.[25]

In Fig. 6(a), the temporal evolution of the electric field is shown for a broadband laser beam with a relative bandwidth $\Delta\omega/\omega_0 = 4.0\%$. The Fourier transform of this electric field can perfectly reproduce the initially assumed flat-top frequency spectrum and random phase spectrum, as shown in Fig. 6(b). In our simulations, the laser beam is propagating along the x direction, and it has a Gaussian transverse profile in the y direction with a spot size w_0. Therefore, the spatial–temporal distribution of the electric field of a broadband laser can be finally expressed as

$$E(t,y) = \exp(-y^2/w_0^2)E(t), \tag{B4}$$

where $E(t)$ is given by Eq. (B3). For a broadband laser beam with a relative bandwidth $\Delta\omega/\omega_0 = 4.0\%$ and a spot size $w_0 = 10\lambda$, the spatial–temporal distribution of its electric field is shown in Fig. 6(c).

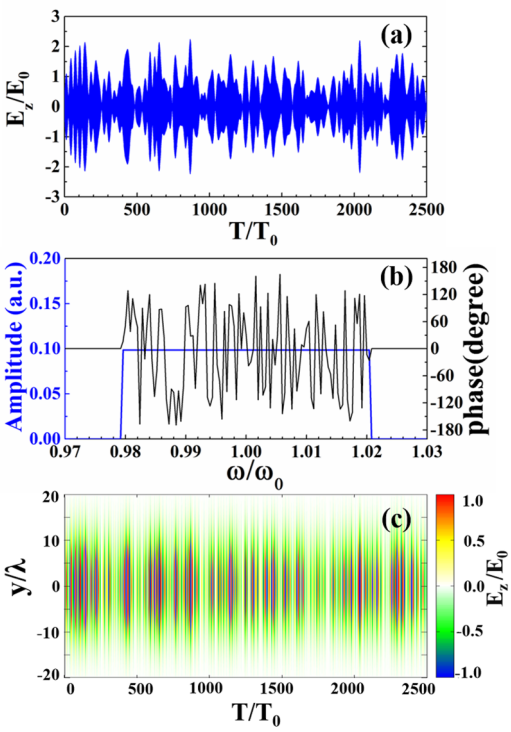

FIG. 6. Model of a broadband laser. (a) The temporal evolution of the electric field obtained from Eq. (B3) for a broadband laser beam with a relative bandwidth $\Delta\omega/\omega_0 = 4.0\%$. (b) Corresponding frequency spectrum and random phase spectrum obtained by Fourier transformation of the electric field in (a). (c) Spatial–temporal distribution of the electric field given by Eq. (B4) for a broadband laser beam with a relative bandwidth $\Delta\omega/\omega_0 = 4.0\%$ and a spot size $w_0 = 10\lambda$.

REFERENCES

[1] R. K. Kirkwood, J. D. Moody, J. Kline, E. Dewald, S. Glenzer, L. Divol, P. Michel, D. Hinkel, R. Berger, E. Williams, J. Milovich, L. Yin, H. Rose, B. MacGowan, O. Landen, M. Rosen, and J. Lindl, "A review of laser–plasma interaction physics of indirect-drive fusion," Plasma Phys. Controlled Fusion **55**, 103001 (2013).

[2] R. S. Craxton, K. S. Anderson, T. R. Boehly, V. N. Goncharov, D. R. Harding, J. P. Knauer, R. L. McCrory, P. W. McKenty, D. D. Meyerhofer, J. F. Myatt, A. J. Schmitt, J. D. Sethian, R. W. Short, S. Skupsky, W. Theobald, W. L. Kruer, K. Tanaka, R. Betti, T. J. B. Collins, J. A. Delettrez, S. X. Hu, J. A. Marozas, A. V. Maximov, D. T. Michel, P. B. Radha, S. P. Regan, T. C. Sangster, W. Seka, A. A. Solodov, J. M. Soures, C. Stoeckl, and J. D. Zuegel, "Direct-drive inertial confinement fusion: A review," Phys. Plasmas **22**, 110501 (2015).

[3] Y.-H. Chen, Z. Li, H. Cao, K. Pan, S. Li, X. Xie, B. Deng, Q. Wang, Z. Cao, L. Hou, X. Che, P. Yang, Y. Li, X. He, T. Xu, Y. Liu, Y. Li, X. Liu, H. Zhang, W. Zhang, B. Jiang, J. Xie, W. Zhou, X. Huang, W. Huo, G. Ren, K. Li, X. Hang, S. Li, C. Zhai, J. Liu, S. Zou, Y. Ding, and K. Lan, "Determination of laser entrance hole size for ignition-scale octahedral spherical hohlraums," Matter Radiat. Extremes **7**, 065901 (2022).

[4] D. S. Montgomery, "Two decades of progress in understanding and control of laser plasma instabilities in indirect drive inertial fusion," Phys. Plasmas **23**, 055601 (2016).

[5] V. T. Tikhonchuk, T. Gong, N. Jourdain, O. Renner, F. P. Condamine, K. Q. Pan, W. Nazarov, L. Hudec, J. Limpouch, R. Liska, M. Krus, F. Wang, D. Yang, S. W. Li, Z. C. Li, Z. Y. Guan, Y. G. Liu, T. Xu, X. S. Peng, X. M. Liu, Y. L. Li, J. Li, T. M. Song, J. M. Yang, S. E. Jiang, B. H. Zhang, W. Y. Huo, G. Ren, Y. H. Chen, W. Zheng, Y. K. Ding, K. Lan, and S. Weber, "Studies of laser-plasma interaction

physics with low-density targets for direct-drive inertial confinement fusion on the Shenguang III prototype," Matter Radiat. Extremes **6**, 025902 (2021).
[6]J. D. Lindl, P. Amendt, R. L. Berger, S. Gail Glendinning, S. H. Glenzer, S. W. Haan, R. L. Kauffman, O. L. Landen, and L. J. Suter, "The physics basis for ignition using indirect-drive targets on the National Ignition Facility," Phys. Plasmas **11**, 339 (2004).
[7]Y. Kato, K. Mima, N. Miyanaga, S. Arinaga, Y. Kitagawa, M. Nakatsuka, and C. Yamanaka, "Random phasing of high-power lasers for uniform target acceleration and plasma-instability suppression," Phys. Rev. Lett. **53**, 1057 (1984).
[8]S. Skupsky, R. W. Short, T. Kessler, R. S. Craxton, S. Letzring, and J. M. Soures, "Improved laser-beam uniformity using the angular dispersion of frequency-modulated light," J. Appl. Phys. **66**, 3456 (1989).
[9]S. N. Dixit, M. D. Feit, M. D. Perry, and H. T. Powell, "Designing fully continuous phase screens for tailoring focal-plane irradiance profiles," Opt. Lett. **21**, 1715 (1996).
[10]B. J. MacGowan, B. B. Afeyan, C. A. Back, R. L. Berger, G. Bonnaud, M. Casanova, B. I. Cohen, D. E. Desenne, D. F. DuBois, A. G. Dulieu, K. G. Estabrook, J. C. Fernandez, S. H. Glenzer, D. E. Hinkel, T. B. Kaiser, D. H. Kalantar, R. L. Kauffman, R. K. Kirkwood, W. L. Kruer, A. B. Langdon, B. F. Lasinski, D. S. Montgomery, J. D. Moody, D. H. Munro, L. V. Powers, H. A. Rose, C. Rousseaux, R. E. Turner, B. H. Wilde, S. C. Wilks, and E. A. Williams, "Laser–plasma interactions in ignition-scale hohlraum plasmas," Phys. Plasmas **3**, 2029 (1996).
[11]E. Lefebvre, R. L. Berger, A. B. Langdon, B. J. MacGowan, J. E. Rothenberg, and E. A. Williams, "Reduction of laser self-focusing in plasma by polarization smoothing," Phys. Plasmas **5**, 2701 (1998).
[12]W. Zheng, X. Wei, Q. Zhu, F. Jing, D. Hu, X. Yuan, W. Dai, W. Zhou, F. Wang, D. Xu, X. Xie, B. Feng, Z. Peng, L. Guo, Y. Chen, X. Zhang, L. Liu, D. Lin, Z. Dang, Y. Xiang, R. Zhang, F. Wang, H. Jia, and X. Deng, "Laser performance upgrade for precise ICF experiment in SG-III laser facility," Matter Radiat. Extremes **2**, 243 (2017).
[13]B. Afeyan and S. Hüller, "Optimal control of laser plasma instabilities using Spike Trains of Uneven Duration and Delay (STUD pulses) for ICF and IFE," EPJ Web Conf. **59**, 05009 (2013).
[14]E. S. Dodd and D. Umstadter, "Coherent control of stimulated Raman scattering using chirped laser pulses," Phys. Plasmas **8**, 3531 (2001).
[15]J. E. Santos, L. O. Silva, and R. Bingham, "White-light parametric instabilities in plasmas," Phys. Rev. Lett. **98**, 235001 (2007).
[16]Y. Zhao, S. Weng, M. Chen, J. Zheng, H. Zhuo, C. Ren, Z. Sheng, and J. Zhang, "Effective suppression of parametric instabilities with decoupled broadband lasers in plasma," Phys. Plasmas **24**, 112102 (2017).
[17]Y. Zhao, S.-M. Weng, H.-H. Ma, X.-J. Bai, and Z.-M. Sheng, "Mitigation of laser plasma parametric instabilities with broadband lasers," Rev. Mod. Plasma Phys. **7**, 1 (2022).
[18]J. J. Thomson and J. I. Karush, "Effects of finite-bandwidth driver on the parametric instability," Phys. Fluids **17**, 1608 (1974).
[19]J. P. Palastro, J. G. Shaw, R. K. Follett, A. Colaïtis, D. Turnbull, A. V. Maximov, V. N. Goncharov, and D. H. Froula, "Resonance absorption of a broadband laser pulse," Phys. Plasmas **25**, 123104 (2018).
[20]A. N. Mostovych, S. P. Obenschain, J. H. Gardner, J. Grun, K. J. Kearney, C. K. Manka, E. A. McLean, and C. J. Pawley, "Brillouin scattering measurements from plasmas irradiated with spatially and temporally incoherent laser light," Phys. Rev. Lett. **59**, 1193 (1987).
[21]H. Y. Zhou, C. Z. Xiao, D. B. Zou, X. Z. Li, Y. Yin, F. Q. Shao, and H. B. Zhuo, "Numerical study of bandwidth effect on stimulated Raman backscattering in nonlinear regime," Phys. Plasmas **25**, 062703 (2018).
[22]R. K. Follett, J. G. Shaw, J. F. Myatt, J. P. Palastro, R. W. Short, and D. H. Froula, "Suppressing two-plasmon decay with laser frequency detuning," Phys. Rev. Lett. **120**, 135005 (2018).
[23]J. W. Bates, J. F. Myatt, J. G. Shaw, R. K. Follett, J. L. Weaver, R. H. Lehmberg, and S. P. Obenschain, "Mitigation of cross-beam energy transfer in inertial-confinement-fusion plasmas with enhanced laser bandwidth," Phys. Rev. E **97**, 061202(R) (2018).
[24]R. K. Follett, J. G. Shaw, J. F. Myatt, C. Dorrer, D. H. Froula, and J. P. Palastro, "Thresholds of absolute instabilities driven by a broadband laser," Phys. Plasmas **26**, 062111 (2019).
[25]H. H. Ma, X. F. Li, S. M. Weng, S. H. Yew, S. Kawata, P. Gibbon, Z. M. Sheng, and J. Zhang, "Mitigating parametric instabilities in plasmas by sunlight-like lasers," Matter Radiat. Extremes **6**, 055902 (2021).
[26]Y. Zhao, S. Weng, M. Chen, J. Zheng, H. Zhuo, and Z. Sheng, "Stimulated Raman scattering excited by incoherent light in plasma," Matter Radiat. Extremes **2**, 190 (2017).
[27]Y. Zhao, Z. Sheng, S. Weng, S. Ji, and J. Zhu, "Absolute instability modes due to rescattering of stimulated Raman scattering in a large nonuniform plasma," High Power Laser Sci. Eng. **7**, E20 (2019).
[28]Y. Zhao, S. Weng, Z. Sheng, and J. Zhu, "Suppression of parametric instabilities in inhomogeneous plasma with multi-frequency light," Plasma Phys. Controlled Fusion **61**, 115008 (2019).
[29]H. Y. Zhou, C. Z. Xiao, J. L. Jiao, Y. Lang, N. Zhao, D. Xie, D. B. Zou, Y. Yin, F. Q. Shao, and H. B. Zhuo, "Kinetic simulation of nonlinear stimulated Raman scattering excited by a rotated polarized pump," Plasma Phys. Controlled Fusion **61**, 105004 (2019).
[30]B. B. Afeyan and E. A. Williams, "Stimulated Raman sidescattering with the effects of oblique incidence," Phys. Fluids **28**, 3397 (1985).
[31]C. R. Menyuk, N. M. El-Siragy, and W. M. Manheimer, "Raman sidescattering in laser-produced plasmas," Phys. Fluids **28**, 3409 (1985).
[32]D. W. Forslund, J. M. Kindel, W. B. Mori, C. Joshi, and J. M. Dawson, "Two-dimensional simulations of single-frequency and beat-wave laser-plasma heating," Phys. Rev. Lett. **54**, 558 (1985).
[33]P. E. Young and K. G. Estabrook, "Angularly resolved observations of sidescattered laser light from laser-produced plasmas," Phys. Rev. E **49**, 5556 (1994).
[34]B. I. Cohen, A. N. Kaufman, and K. M. Watson, "Beat heating of a plasma," Phys. Rev. Lett. **29**, 581 (1972).
[35]B. I. Cohen, M. A. Mostrom, D. R. Nicholson, A. N. Kaufman, C. E. Max, and A. Bruce Langdon, "Simulation of laser beat heating of a plasma," Phys. Fluids **18**, 470 (1975).
[36]C. Z. Xiao, H. B. Zhuo, Y. Yin, Z. J. Liu, C. Y. Zheng, and X. T. He, "Linear theory of multibeam parametric instabilities in homogeneous plasmas," Phys. Plasmas **26**, 062109 (2019).
[37]W. Kruer, *The Physics of Laser Plasma Interactions* (CRC Press, 2019).
[38]T. M. Antonsen, Jr. and P. Mora, "Self-focusing and Raman scattering of laser pulses in tenuous plasmas," Phys. Fluids B **5**, 1440 (1993).
[39]T. D. Arber, K. Bennett, C. S. Brady, A. Lawrence Douglas, M. G. Ramsay, N. J. Sircombe, P. Gillies, R. G. Evans, H. Schmitz, A. R. Bell, and C. P. Ridgers, "Contemporary particle-in-cell approach to laser-plasma modelling," Plasma Phys. Controlled Fusion **57**, 113001 (2015).
[40]L. Yin, B. J. Albright, K. J. Bowers, W. Daughton, and H. A. Rose, "Saturation of backward stimulated scattering of laser in kinetic regime: Wavefront bowing, trapped particle modulational instability, and trapped particle self-focusing of plasma waves," Phys. Plasmas **15**, 013109 (2008).
[41]Q. K. Liu, E. H. Zhang, W. S. Zhang, H. B. Cai, Y. Q. Gao, Q. Wang, and S. P. Zhu, "Non-linear stimulated Raman back-scattering burst driven by a broadband laser," Phys. Plasmas **29**, 102105 (2022).
[42]C. Z. Xiao, H. B. Zhuo, Y. Yin, Z. J. Liu, C. Y. Zheng, Y. Zhao, and X. T. He, "On the stimulated Raman sidescattering in inhomogeneous plasmas: Revisit of linear theory and three-dimensional particle-in-cell simulations," Plasma Phys. Controlled Fusion **60**, 025020 (2018).
[43]R. K. Follett, J. G. Shaw, J. F. Myatt, H. Wen, D. H. Froula, and J. P. Palastro, "Thresholds of absolute two-plasmon-decay and stimulated Raman scattering instabilities driven by multiple broadband lasers," Phys. Plasmas **28**, 032103 (2021).
[44]G. Cristoforetti, L. Antonelli, D. Mancelli, S. Atzeni, F. Baffigi, F. Barbato, D. Batani, G. Boutoux, F. DÁmato, J. Dostal, R. Dudzak, E. Filippov, Y. J. Gu, L. Juha, O. Klimo, M. Krus, S. Malko, A. S. Martynenko, P. Nicolai, V. Ospina, S. Pikuz, O. Renner, J. Santos, V. T. Tikhonchuk, J. Trela, S. Viciani, L. Volpe, S. Weber, and L. A. Gizzi, "Time evolution of stimulated Raman scattering and two-plasmon decay at laser intensities relevant for shock ignition in a hot plasma," High Power Laser Sci. Eng. **7**, E51 (2019).

[45]Y. Ji, C.-W. Lian, R. Yan, C. Ren, D. Yang, Z.-H. Wan, B. Zhao, C. Wang, Z.-H. Fang, and J. Zheng, "Convective amplification of stimulated Raman rescattering in a picosecond laser plasma interaction regime," Matter Radiat. Extremes **6**, 015901 (2021).
[46]D. Froula, R. K. Follett, C. Dorrer, J. Bromage, E. M. Hill, B. E. Kruschwitz, J. P. Palastro, and D. Turnbull, "Fourth-generation laser for ultra-broadband experiments-expanding inertial confinement fusion design space through mitigation of laser-plasma instabilities," in APS Division of Plasma Physics Meeting Abstracts, 2019.
[47]Y. Gao, Y. Cui, L. Ji, D. Rao, X. Zhao, F. Li, D. Liu, W. Feng, L. Xia, J. Liu, H. Shi, P. Du, J. Liu, X. Li, T. Wang, T. Zhang, C. Shan, Y. Hua, W. Ma, X. Sun, X. Chen, X. Huang, J. Zhu, W. Pei, Z. Sui, and S. Fu, "Development of low-coherence high-power laser drivers for inertial confinement fusion," Matter Radiat. Extremes **5**, 065201 (2020).